Contents lists available at GrowingScience

Engineering Solid Mechanics

homepage: www.GrowingScience.com/esm

# Deformation of laboratory truncated disc samples with stress concentrators

**L.B. Tsvik [a,b], E.V. Zenkov [a,b*], D.A. Elovenko[b] and D.O. Malomigev[a]**

[a]*Department of Carriages and Carriage Facilities, Irkutsk State Transport University, 15, Chernishevskogo, Irkutsk, 664074, Russian Federation*
[b]*Department of Mechanics and Strength of Materials, Irkutsk National Research Technical University, 83, Lermontov, Irkutsk, 664074, Russian Federation*

**ARTICLEINFO**

*Article history*:
Received 19 June 2024
Accepted 26 October 2024
Available online
26 October 2024

*Keywords*:
*Disk samples with grooves*
*Fracture of disk samples*
*Variant studies*
*Strength of truncat-ed disks*
*Cracking of truncated discs*
*Failure of steel 45 under biaxial tension*

**ABSTRACT**

The article assesses the structural strength of sample materials destroyed on standard equipment for determining the mechanical properties of materials. The distribution of mechanical stresses of laboratory disk samples with stress concentrators in the form of grooves on the support surfaces was analyzed. It was revealed that the disc truncation along the two symmetrical chords allows for varying the type of stress state in the sample and intensity of stresses in the working zone. The problems of the linear theory of elasticity were solved for samples with different degrees of disc truncation and with different geometric parameters of the groove profile. The analysis of disk deformation showed that these laboratory samples can be used in simulating the type and level of stress state of various parts of machines and mechanisms. This factor significantly expands the possibilities for assessing the structural strength of materials during laboratory studies of the materials. It was revealed that the type of stress state plays a role in localizing the sources of destruction of highly loaded structural elements made from structural carbon steel St45. The results can be used both for the experimental assessment of the structural strength of materials and for constructing limit state equations corresponding to a stress state level and type.



## 1. Introduction

Highly loaded structural elements can be subjected to a set of static or cyclic loads that create a three-dimensional distribution of mechanical stresses (DMS) marked by a significant concentration of stress in places of structural inhomogeneities (holes, protrusions, grooves, cutouts). The DMS that occurs near these zones determines the service life of structures both under static and cyclic loading or under brittle fractures (Kogaev et al., 1985; Smirnov-Alyaev, 1968; Tsvik et al., 1978; Pisarenko et al., 2008; Lebedev & Kovalchuk, 2003; Koutiri et al., 2018; Matake, 1977; Makhutov, 1981; Makhutov, 2005; Sines et al., 1959; Berto et al., 2015; Leevers et al., 1976; Bellett, Morel, Morel, & Lebrun, 2011; Tsvik & Zenkov, 2022; Yosri et al., 2021). It is important that with different types of stress state – compression, tension, or shear – and with complex types of stress state, which are a combination of the three types, the strength conditions of structural elements can significantly vary (Smirnov-Alyaev, 1968; Tsvik et al., 1978). This factor creates the need to apply combined strength criteria using generalized limit state equations for materials under static loads (Kogaev et al., 1985; Pisarenko et al., 2008; Lebedev & Kovalchuk, 2003; Zenkov & Tsvik, 2015; Zenkov & Tsvik, 2018; Tsvik & Zenkov, 2022) or to use fatigue curves obtained under cyclic loading for a given type of stress state and stress concentration in a potential source of destruction of a real structure.

The static structural strength (Kogaev et al., 1985; Matake, 1977; Makhutov, 1981; Makhutov, 2005; Bondar et al., 2024) of the material can be calculated taking into account the type of stress state using various limit state equations, such as the Drucker-Prager equation, the Pisarenko-Lebedev equation, or the Yagna-Buzhinsky equation (Kogaev, Makhutov, & Gusenkov, 1985; Keller & Petukhov, 2020; Drucker & Prager, 1952).

* Corresponding author.
E-mail addresses: jovanny1@yandex.ru (D.O. Malomigev)

ISSN 2291-8752 (Online) - ISSN 2291-8744 (Print)

doi: 10.5267/j.esm.2024.10.002

For uniaxial tension in the source of possible destruction of the structural element, standard materials are used (GOST 1497-84, 2008). For the complex type of stress state, the researchers (Zenkov & Tsvik, 2018; Tsvik & Zenkov, 2022; Zenkov & Tsvik, 2017) developed a method for assessing the structural strength based on the results of destruction of special laboratory samples that have similar types of stress state in the source of their destruction and in the source of possible destruction of the structural element. The samples can be tested to failure on the standard equipment for determining the mechanical properties of materials (Tsvik, 2017; Tsvik et al., 2020; Tsvik & Zenkov, 2022). The methodology can be employed on complex laboratory equipment (Zenkov & Tsvik, 2018). Significantly, the testing process can become more complicated (Zenkov & Tsvik, 2018; Tsvik & Zenkov, 2022; Zenkov & Tsvik, 2017; Tsvik, 2017).

The approach, which takes into account the type of stress state in areas of possible destruction of the structural element, involves the following steps:

1) computational modeling of the level and type of stress state in the structural element under operation conditions;
2) determination of the DMS calculated values of components included in the combined strength criterion of material in possible sources of their destruction;
3) assessment of the structural strength of the materials by testing laboratory samples to failure with a given ratio of stress state invariants determined at stage 2.

At the first and second stages, the problems of deformation mechanics are solved using numerical methods. At the second stage, the characteristics of the type of stress state in the source of destruction of the structure are determined (Zenkov et al., 2019). In accordance with the methodology (Zenkov & Tsvik, 2018; Tsvik & Zenkov, 2022; Zenkov & Tsvik, 2017), the third stage of assessing the structural strength can be implemented if there are appropriate laboratory samples for mechanical tests, the value of stress state invariants at the moment of destruction coincides with the values of the type of stress state determined at the second stage using computer technology.

$P$ (the coefficient of the type of stress state), which characterizes the type of stress state equal to the ratio (1), is used as a criterion for the similarity of stress state in the structures and in the corresponding samples used for mechanical tests (Kogaev et al., 1985; Smirnov-Alyaev, 1968; Pisarenko et al., 2008; Tsvik & Zenkov, 2022),

$$P = \frac{I_1}{\sigma_i}, \tag{1}$$

where $I_1$ are the first invariant of the stress tensor; $\sigma_i$ is the equivalent stress determined as

$$\sigma_i = \frac{1}{\sqrt{2}}\sqrt{(\sigma_1-\sigma_2)^2+(\sigma_1-\sigma_3)^2+(\sigma_2-\sigma_3)^2}\ . \tag{2}$$

Stress concentration coefficient $K_\sigma$ was also used as a criterion for the similarity of DMS in the analyzed structures and corresponding samples used for mechanical testing

$$K_\sigma = \frac{\sigma_i^{\max}}{\sigma_i^{ном}}, \tag{3}$$

where $\sigma_i^{max}$ is the maximum stress intensity in the source of destruction of the laboratory sample; $\sigma_i^{nom}$ is the nominal stress intensity in the center of the (in diameter and thickness) similarly loaded disk sample without stress concentrators on its sides. While strength testing, it is sometimes necessary to take into account the scale factor that determines the strength of highly loaded large-sized structures (Kogaev et al., 1985; Tsvik & Zenkov, 2022).

In the general case, $P$, which characterizes the type of stress state in the centers of destruction of highly loaded structural elements, can significantly varies. An example of the influence (Smirnov-Alyaev, 1968) of the type of stress state for $P < 0$ (this state occurs when the principal stresses are negative at the observation point) is the calculated strength of the contact zone of the rolling body of the axle box bearing of railway cars (Tsvik, Tarmaev, & Bocharov, 2019). In this case, $P$ is negative, close to –2, and for steel ShKh4 used for the manufacture of bearings, the standard permissible contact stresses are equal to 3500 MPa (Tsvik & Zenkov, 2022), which is more than twice the tensile strength of this steel under uniaxial stretching. In the contact zone of the railway wheel and the rail (Krotov & Kononov, 2022), the contact stresses are also significant. The experiments that revealed an opposite effect – a decrease in the strength of the material under biaxial tension – are described in (Bellett et al., 2011; Zenkov & Tsvik, 2018; Vilimok et al., 2013; Tsvik & Zenkov, 2022). The specified features of the structural strength of materials of critical structures create the need to study standard samples for mechanical

testing to failure, simulating the real type and level of stress state within a wide range of P and $K_\sigma$ values. To assess both the static and cyclic strength under complex stress-strain conditions, samples with various configurations can be used (Bellett et al., 2011; GOST 25.504-82, 2004; GOST 25.506-85, 1985). In (Bellett, Morel, Morel, & Lebrun, 2011; Mathiak et al., 1992), complex shaped-samples were used for mechanical testing – plates of variable thickness with through cutouts and axisymmetric notches. In some cases, samples in the form of plates of variable thickness located inside the rigid circular rim and the reverse curvature rim were used (Keller & Petukhov, 2020) (Fig. 1).

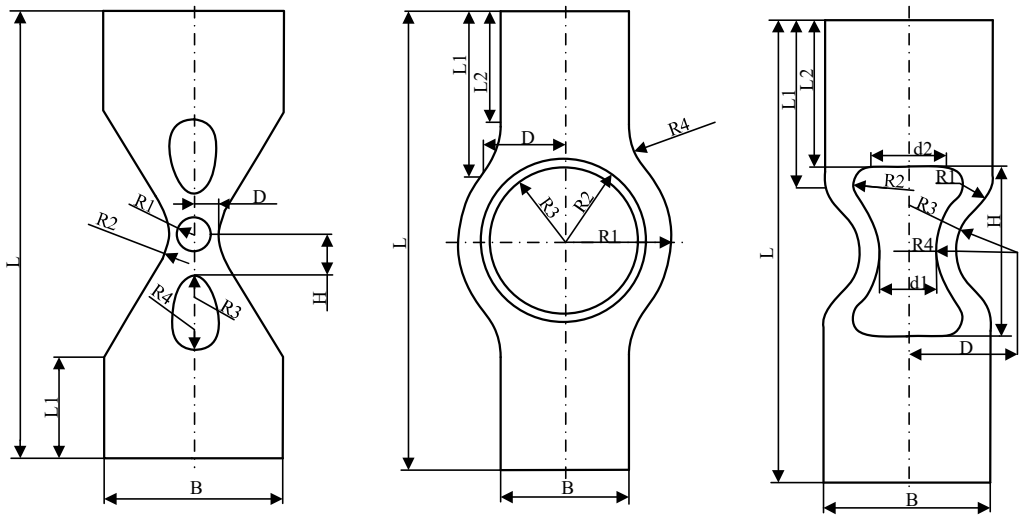


a) b) c)

**Fig. 1.** The diagrams of the samples:
a) Plate-shaped sample of variable thickness with a spherical recess in its central part
b) and c) Plate-shaped samples of variable thickness with a rigid circular rim

The samples in Fig. 1 have complex spatial shapes. The samples are tested under uniaxial tension (their uniaxial compression is hampered due to the possible loss of stability of plate-shaped samples during compression). This factor and the scheme of uniaxial loading of samples limit the possibility of modeling *P*. The present study analyzed the dependence of stress state on the geometric parameters of disk samples described in (Leevers et al., 1976). They have a simple configuration and allow for simulating a wide range of changes in *P* and $K_\sigma$.

## 2. The calculation scheme and the methods for studying disk samples

The specified quantitative stress state analysis (**Figs. 2–5** (Tsvik, 2017; Tsvik et al., 2020)) should take into account both physical (Kachanov, 2004) and geometric (Lurie, 2012) nonlinearities of deformation. This approach is used for assessing (Oden, 1976; Rychkov, 2013) the deformation of samples destroyed while testing.

For an approximate stress state assessment, the relations of the linear theory of elasticity were used depending on the geometric parameters of the samples (Zenkov & Tsvik, 2022)

$$\boldsymbol{L}\mathbf{u} = (\lambda + \mu)\, grad\, div\, \mathbf{u} + \mu \Delta \mathbf{u} = 0. \tag{4}$$

Eq. (4) were solved under conditions (Zenkov & Tsvik, 2022)

$$(\mathbf{v}\cdot\mathbf{T})\Big|_{S_\sigma} = \mathbf{F}(M),\ M \in S_\sigma;\ (\mathbf{u}\cdot\mathbf{v})\Big|_{S_{u\sigma}} = 0;\ (\mathbf{v}\cdot\mathbf{T}\cdot\boldsymbol{\tau})\Big|_{S_{u\sigma}} = 0,\quad M \in S_{u\sigma}. \tag{5}$$

In addition to conditions (5), which determine the boundary conditions on various sections of surface S, conditions on some lines of this surface corresponding to the fixation of the sample in space are also specified.

The sample in **Figs. 2–5** (Tsvik, 2017; Tsvik et al., 2020) is a part of the circular disk of constant thickness (base disk) formed by truncation of the base disk by two planes (**Fig. 2**). The sample has a bearing surface, a loading surface and a groove located on one of these surfaces. While testing, the sample is supported along the outer edge of the support surface (in **Figs. 2, 3**, it is supported along the outer edge of the lower surface of the sample). The shape of the samples is a generalization of

the shape of beams with stress raisers in the form of grooves (**Fig. 2**), used to assess the strength of materials under three-point bending of beams (GOST 25.506-85, 1985).

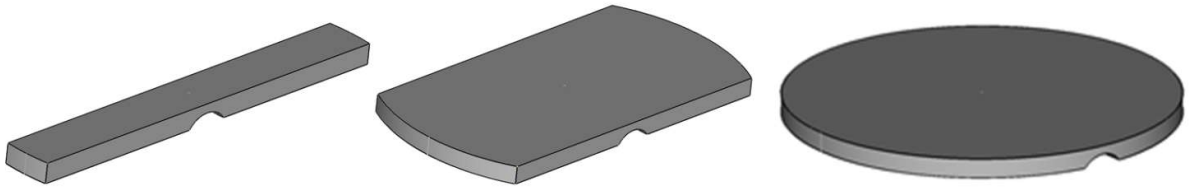

a) b) c)

**Fig. 2.** The diagram of the truncated disk sample
a), b) and c) truncation degrees

While computational modeling, it is assumed that during the mechanical testing the sample is supported in accordance (Tsvik & Zenkov, 2022) (in **Figs. 2–4**, the support side is the lower side of the circular plate). **Fig. 3** shows the samples with different cross-sectional shapes of concentrating grooves and their ring supports. The samples have two planes of symmetry (in **Fig. 4**, the surfaces are shaded), which allows us to further analyze only a quarter of the sample rather the entire sample (**Fig. 5**).

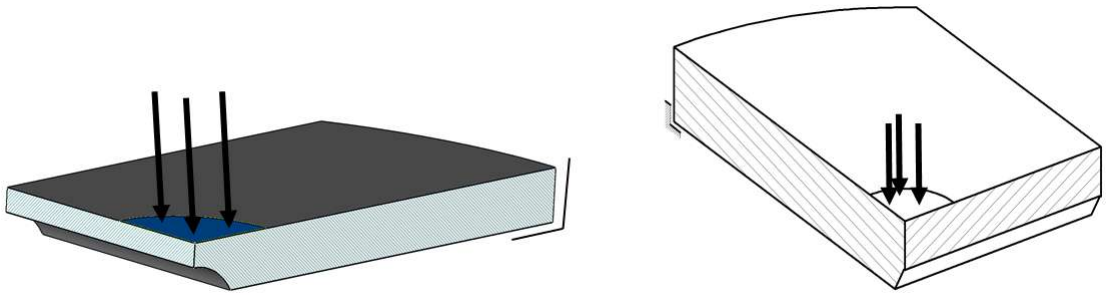

a) b)

**Fig. 3.** Loading of a truncated disk specimen during strength testing:
a) concentrating groove with an arcuate cross-section profile
b) concentrating groove with a V-shaped cross-sectional profile

To identify the patterns of deformation of the samples, the finite element (FE) stress state modeling was performed (Tsvik & Zenkov, 2022). Values of the geometric parameters varied (**Fig. 4**). Disk samples with an arcuate cross-sectional profile of the grooves, an outer diameter of 200 mm, and a disk thickness of 10 mm were analyzed. The values of the following dimensionless quantities varied

$$\rho = \frac{r}{H} \in [1{,}1;\ 2{,}1];\ \eta = \frac{h}{H} \in [0{,}1;\ 0{,}9];\ \delta = \frac{s}{D} \in [0{,}4;\ 1]. \tag{6}$$

$H$ is the total thickness of the sample, $D$ is the outer diameter of the sample, $r$ is the radius of the groove surface rounding, $h$ is the groove depth, $s$ is the width of the truncated disk (**Fig. 4**), $\rho$, $\eta$ and $\delta$ are the relative values of $r$, $h$ and $s$. The cross-sectional shapes of the concentrating grooves can be different (e.g., U-, V- or arc-shaped), which allows the samples to be used in the experimental assessment of various characteristics of the structural strength: crack resistance, static or cyclic strength of materials.

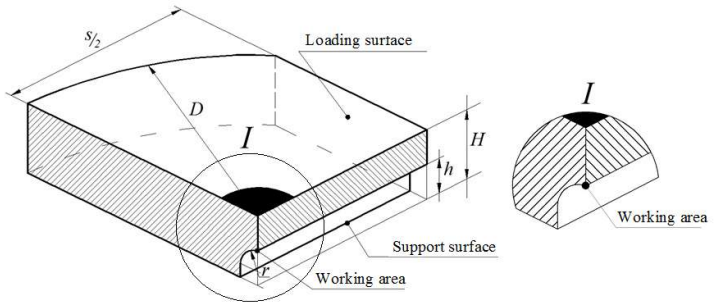


**Fig. 4.** Truncated disk sample and its working area (*I*)

The DMS of the disk samples were analyzed using the FE modeling results with Femap. The necessary conditions for fixing and loading the samples were carried out in accordance with (Tsvik & Zenkov, 2022) (**Fig. 5**).

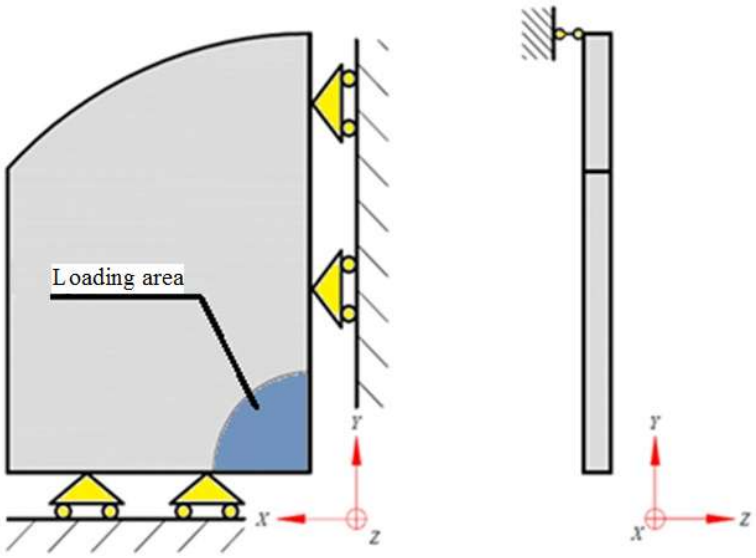


**Fig. 5.** The scheme of fastening and loading disk samples

To ensure the required accuracy of computational modeling, FE breakdown thickening was localized (Zenkov et al., 2011; Tsvik et al., 2017). For this purpose, the area under consideration (a quarter of the disk) was considered as a system of fragments divided into FEs independently of each other. The fragments adjacent to the working area of the sample were divided into smaller FEs. The dimensions of the FE mesh cells within one fragment changed following the law of progression. The accuracy of the results was assessed using a sequence of FE splits, in which the largest size of the FE within the fragments was halved. The solution of test problems ((Zenkov et al., 2011; Peterson, 1977; Neuber, 1947), qualitatively close to the one under consideration, showed that the error in FE approximations of $\sigma i^{max}$ can be estimated from the relative closeness of $\sigma i^{max}$ values in two successive approximations. The computational modeling error did not exceed 5%. The total number of truncated FE disks used in the discretization was one million.

## 3. Results of the computational stress state modeling for disk samples with an arcuate cross-section profile

The localization of the source of destruction in the samples is determined by the localization of the maximum value of stress intensity $\sigma i^{max}$ that occurs when they are loaded with a test force, as well as by features of the distribution of $P$ values – the stiffness coefficient of the type of stress state (Smirnov-Alyaev, 1968; Lebedev & Kovalchuk, 2003; Zenkov & Tsvik, 2015). When in the zone of maximum $\sigma_i$ $P$ is relatively small, the localization of the source of destruction may not coincide with the localization of $\sigma_i^{max}$ (Tsvik et al., 1978; Peterson, 1977; Tsvik et al., 1993). To choose design options for truncated disks in which the localization $\sigma_i^{max}$ and maximum $P$ coincide (in these samples the localization of the source of destruction is determined unambiguously), the dependence of $P$ on the main geometric parameters of truncated disks with concentrating grooves was simulated. While computational modeling, the values of the main DMS characteristics required to assess the strength of the material – $P$ and $K_\sigma$ – were determined. **Fig. 6** shows the distribution of $\sigma_i$ for one of the design options of the disk samples.

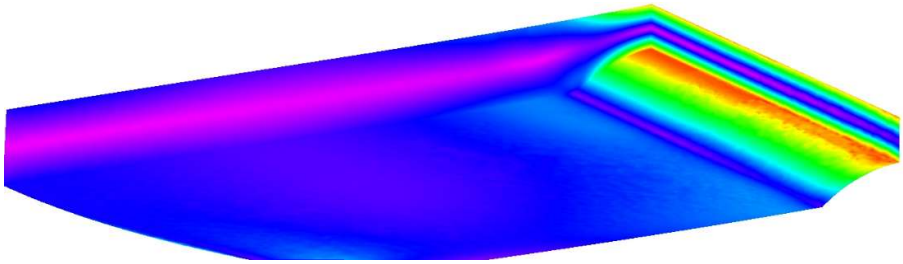

**Fig. 6.** Distribution of the value $\sigma_i$ in the disk sample
with $\rho = 1{,}9$; $\eta = 0{,}4$; $\delta = 0{,}55$; $P = 1{,}5$; $K_\sigma = 4{,}5$

The computational modeling results are presented in **Fig. 7–9**. They show that the truncated disk samples make it possible to simulate biaxial tension characterized by $P$ in a wide practically significant range of values [0; 2]) at different values of $K_\sigma$. Fatigue strength studies show that it is determined not only by the level and type of stress state in the potential source of

destruction, but also by $K_\sigma$ (de Oliveira Miranda et al., 2019). The use of the truncated disk samples allows us to vary both $P$ and $K_\sigma$ (**Fig. 7**).

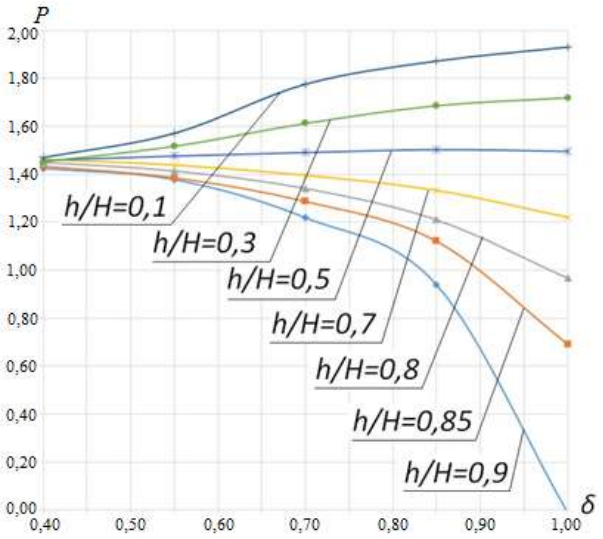


**Fig. 7**. Dependence of P on truncation parameter δ at radius ρ = 1,9

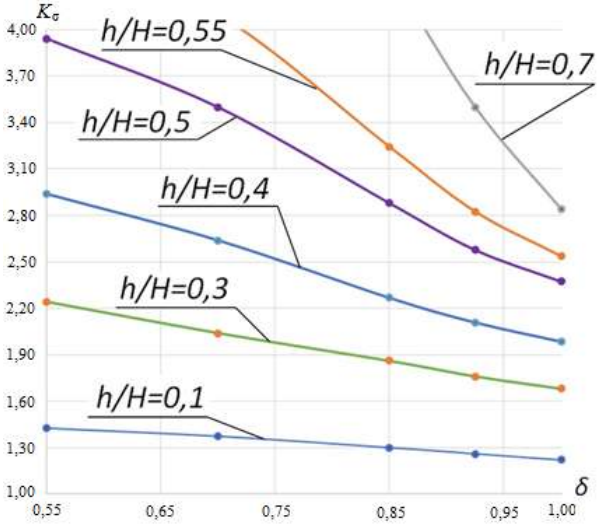


**Fig. 8.** Dependence of $K_\sigma$ on truncation parameter δ at radius ρ = 1,9

The computational modeling revealed the dependence of $P$ and $K_\sigma$ on ρ, η and δ. Each of the ranges (6) was divided into 4–6 intervals. Examples of the dependencies for some design parameters are presented in **Fig. 7-8**. They present the calculated distributions of $P$ and $K_\sigma$ of the disk samples depending on truncation parameter δ and groove depth η with groove profile radius ρ equal to 1.9. The results show that $P$ and $K_\sigma$ vary in the range of

$$0 \le P \le 2; \;\; 1{,}2 < K_\sigma < 4. \qquad (7)$$

If necessary, concentrating grooves of the level of DMS can be located on the loading surface of the samples, which makes it possible to study the structural strength of materials under compression. This deformation feature significantly expands the possibilities of studying and assessing the structural strength. The results presented in **Fig. 7** show that as the groove deepens, the nature of the dependence of $P$ on δ changes significantly. For relatively small groove depths (η ∈ [0.1, 0.5]) with increasing δ, $P$ increases from 1.5 to 2. When the groove reaches the middle surface of the base disk (η = 0, 5), $P$ is independent of the truncation degree and close to 1.5 (**Fig. 9**; the data presented in **Fig. 9** correspond to the dependencies shown in **Fig. 7**). With an increase in η, $P$ decreases with increasing δ, reaching $P = 0$.

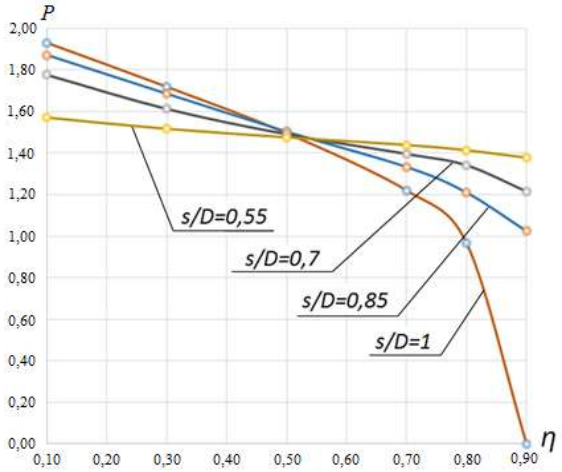


**Fig. 9.** Dependence of $P$ on depth $\eta$

Structural strength assessment involves the modeling of the stress concentration level in the source of possible destruction (GOST 25.502-79, 1979) ($K_\sigma$ modeling). The computational modeling results for $K_\sigma$ depending on η and δ are presented in Fig. 10, and the dependences of $P$ and $K_\sigma$ on groove profile radius ρ and truncation parameter δ for the fixed value of groove

depth η = 0.9 – in **Fig. 11**. For fixed values of η, *P* changes slightly with a change in the degree of truncation δ (Fig. 10,a). As shown below, in a number of important cases, this factor makes it possible to simultaneously simulate both the similarity parameter of the type of stress state (*P*) and the required value of $K_\sigma$ using the samples for mechanical testing.

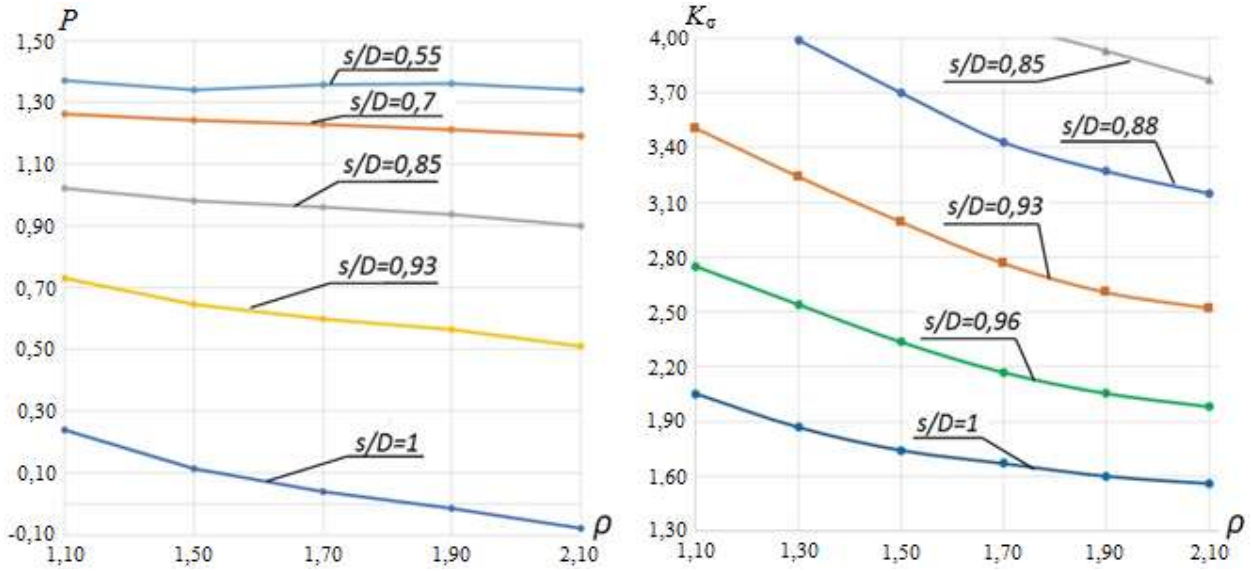


a) b)

**Fig. 10.** Dependence a) of *P* and b) $K_\sigma$ on radius ρ at depth $\eta = 0,9$

The results presented in **Fig. 7–11** show that the disk samples with concentrating grooves make it possible to simulate DMS in which *P* varies from 1 to 0. This property makes it possible to study the crack resistance of materials (GOST 25.506-85, 1985) for complex stress state corresponding to the specified range. To implement this approach, it is necessary to create a fatigue crack of a controlled size on the surface of the concentrating groove with an arcuate cross-section profile.

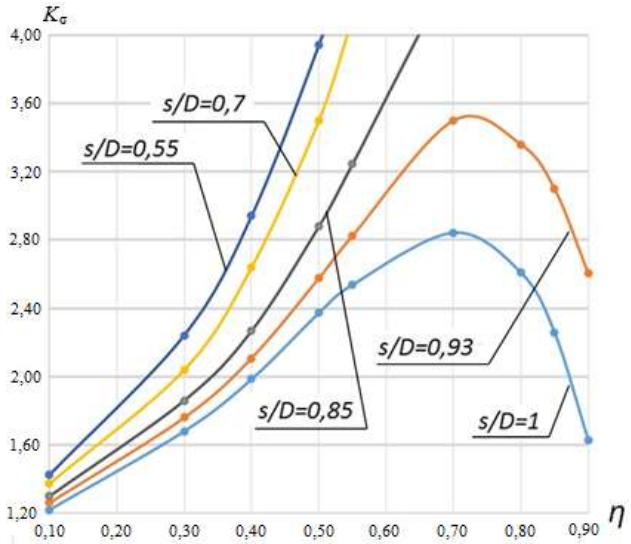


**Fig. 11**. Dependence of $K_\sigma$ on groove depth η and truncation degree δ at radius ρ = 1,9

Consider the application of the identified patterns and the obtained numerical results for the truncated disk samples. Choose a structural element in the complex stress state with P = 1.5 and $K_\sigma = 3$. To solve this problem, it is necessary identify the dependence of P and $K_\sigma$ on the geometric parameters of the truncated disk samples in the appropriate range of these parameters using the numerical methods. For this purpose, the dependences of P and Kσ on ρ, η and δ can be used. First, groove radius *r* is chosen. Let the dimensionless value of groove surface radius *ρ* be 1.9. Second, the required groove depth *h* is determined. According to the dependencies shown in **Fig. 7**, select the dimensionless value of groove depth $\eta = 0.5$, which corresponds to $P = 1.5$. Finally, choose the required value of disk truncation parameter *S*. Choose the dimensionless value of disk truncation parameter $\delta = 0.82$ using the dependencies presented in Fig. 6 and based on $\eta = 0.5$ and $\rho = 1.9$. The accuracy of this assessment

is ensured by identical values of the similarity parameters – similarity of the stress state in the possible source of destruction of the structural element with $P = 1.5$ and $K_\sigma = 3$ and the stress state in the working area of the chosen disk sample.

For various highly loaded elements in the complex stress state, it is necessary to perform preliminary computational modeling and construct various dependencies similar to those presented in **Figs. 7–11** corresponding to the specified DMS. Truncated disk samples chosen in accordance with the algorithm described above make it possible to simulate the factors that determine the strength of $P$ and $K_\sigma$ simultaneously already at the stage of laboratory studies. It is important that dependencies similar to those presented in **Figs. 7–11** can be obtained for different values of thickness of the base disk $H/D$. The choice of ρ, η and δ becomes more free.

The position of the source of destruction of structural elements of highly loaded parts of machines, devices and mechanisms is of practical interest. When the localization zones of maximum $P$ and $K_\sigma$ coincide, the position of the source of destruction is obvious: the coincidence point is the source of destruction of the structural element. If the zones do not coincide (Tsvik, Pimshtein, & Borsuk, 1978; Tsvik et al., 1993), the localization of the source of destruction is determined by the calculation and experimental methods (Zenkov & Tsvik, 2015; Zenkov & Tsvik, 2018).

Within the above approach, geometrically identical disk samples from structural carbon steel St45 were manufactured and brought to destruction (GOST 1050-2013, 2014). While testing, the samples were divided into two groups of three samples and loaded in accordance with the diagram presented in **Fig. 3**. While testing, INSTRON 5989 was used. The choice of this steel grade was determined by the following. The specified steel can be subjected to hardening, which allows increasing its tensile strength to relatively high values: 800 - 850 MPa. This circumstance allows using it for the manufacture of units and parts subject to high operational loads. At the same time, the residual elongation at break of this steel reaches 12-14%. It is of interest to study the nature of the destruction of this steel under biaxial tension.

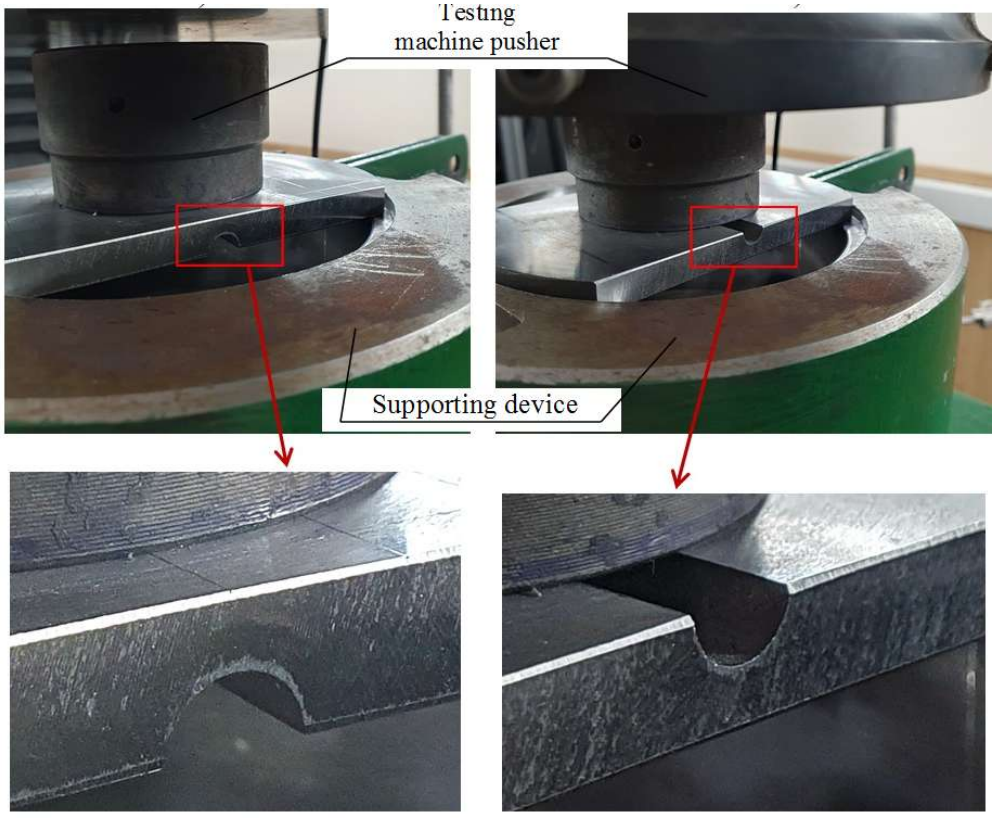


a) b)

**Fig. 12.** Placement of the truncated disk samples in the supporting device of the testing machine:
a) Concentrating groove is located on the support surface of the samples
b) Concentrating groove is located on the loading surface of the samples

In the first group, the tested samples were placed in the supporting device of the testing machine so that the concentrating groove was located on the supporting side of the samples (**Fig. 12, a**). In the second group, they were placed on the loading side (**Fig. 12, b**). $K_\sigma$ values in both groups were almost similar and equal to 3.75. The values were obtained during the qualitative analysis of sample deformation using the linear theory of elasticity. In the first group, on the groove surface, σ1

was positive, and $P$ = 1.5 (the DMS on the groove surface on the axis of rotation of the base disk was relatively “hard” (Smirnov-Alyaev, 1968). The ratio – maximum $P$ and $K_\sigma$ achieved at the same point of the test sample.

In the second group of samples, $\sigma_1$ on the groove surface was negative; P was also negative and equal to –1.4 (the DMS on the groove surface is “softer” (Smirnov-Alyaev, 1968) than in the first group).

The destruction of the samples showed that in the first group the source of destruction was located on the surface of the concentrating groove (**Fig. 13**). The destruction of the samples from the first group (**Fig. 12, a**) began with the occurrence of cracks 3–7 mm long on the surface of the concentrating groove (in its middle part) (**Fig. 13, b**). The test force was equal (on average for the group) to 45±1 kN. Then, the test force decreased (**Fig. 14**), and the process was accompanied by a significant change in the shape of the sample, followed by its division into parts (**Fig. 13, c**). It should be noted that the fracture surface of the samples of this group has a matte color, corresponds to the macrobrittle nature of the fracture and is located perpendicular to the direction of maximum tensile stresses (**Fig. 13, d**).

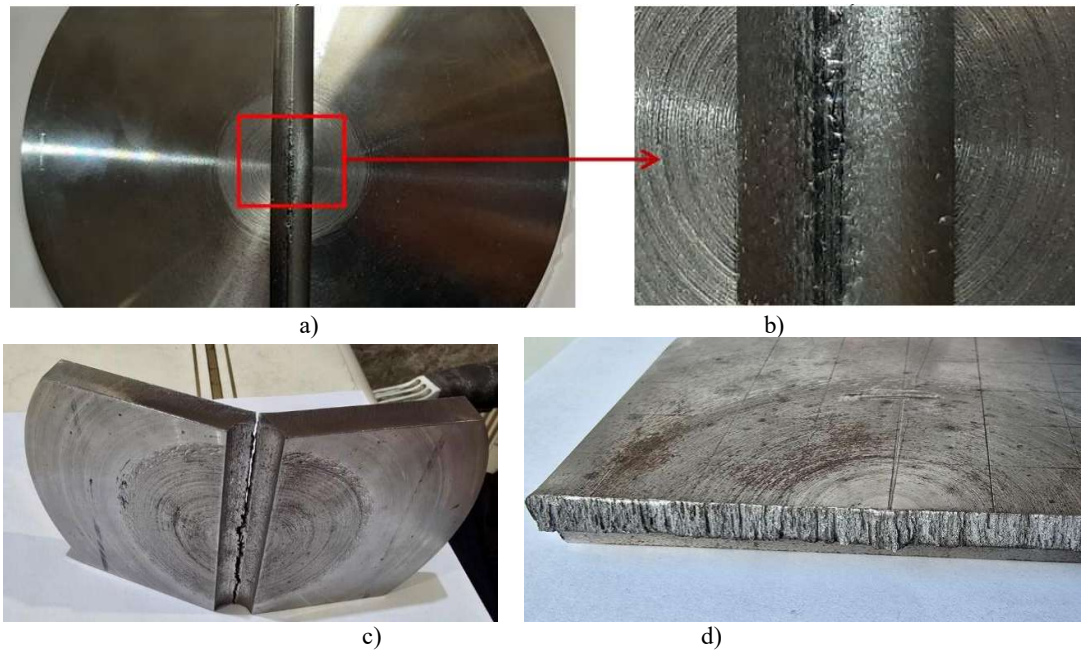


**Fig. 13.** The destroyed truncated disk sample from the first group:
a) crack localization b) crack initiation c) division of the sample into parts d) fracture surface

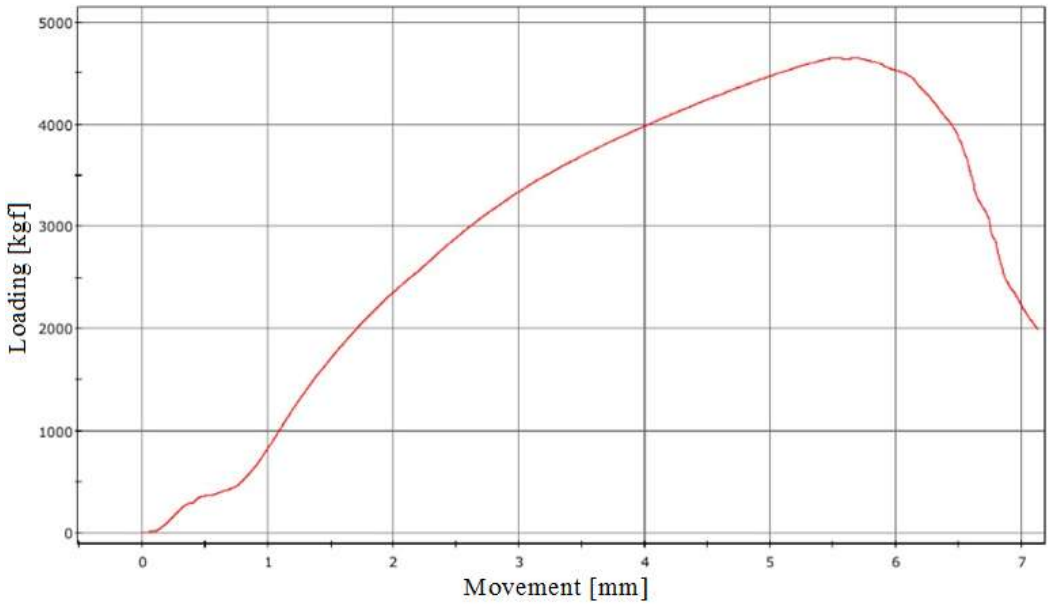


**Fig. 14.** The loading diagram for the truncated disk samples from the first group

In the second group (**Fig. 12(b)**), the source of destruction was located on the support surface of the samples in its central part (**Fig. 15(b)**). The destruction of the samples began at a test force equal to (on average for the group) 87±2 kN. The destruction process was accompanied by a significant change in the shape of the sample and its division into parts (Fig. 15(c)), which occurred with a decrease in the test force (**Fig. 16**). It should be noted that the fracture surface of the samples of this group has a character similar to the fracture surfaces of the samples of the first group (**Fig. 15, d**). This allows us to conclude that the fracture of the steel under consideration at values of $P$ = 1.4-1.5 has a brittle character, which limits the possibilities of its use under cyclic loading conditions at such values of $P$.

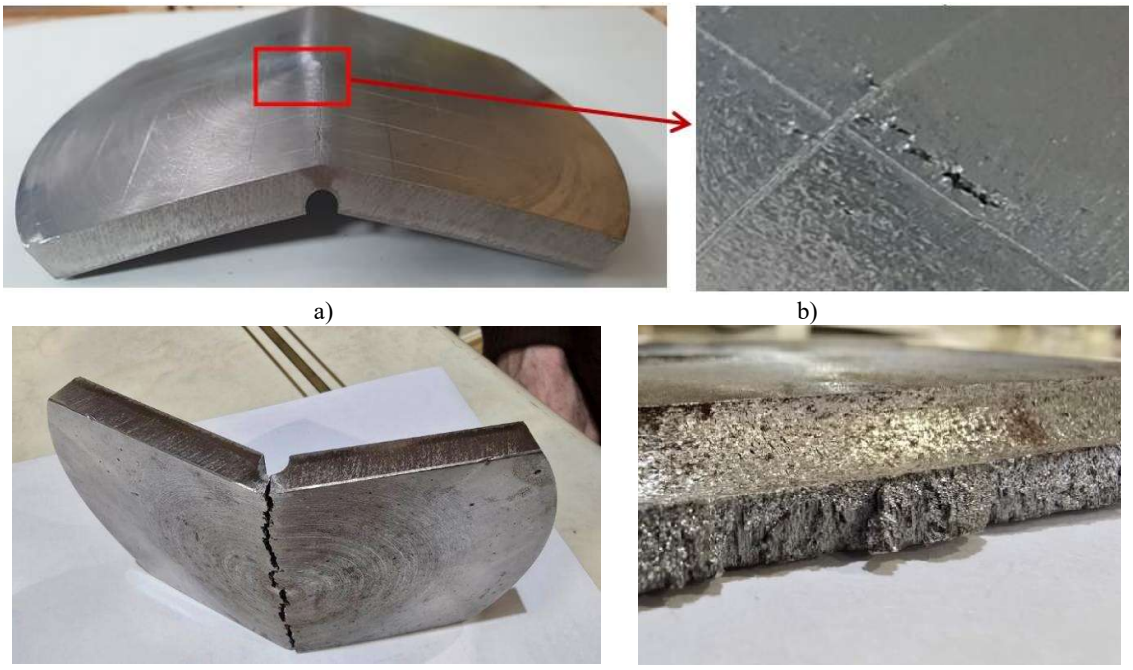

a) b) c) d)

**Fig. 15.** Occurrence and development of the crack on the bearing surface in the truncated disk sample from the second group:
a) localization of the crack b) occurrence of the crack
c) division of the sample into parts d) fracture surface

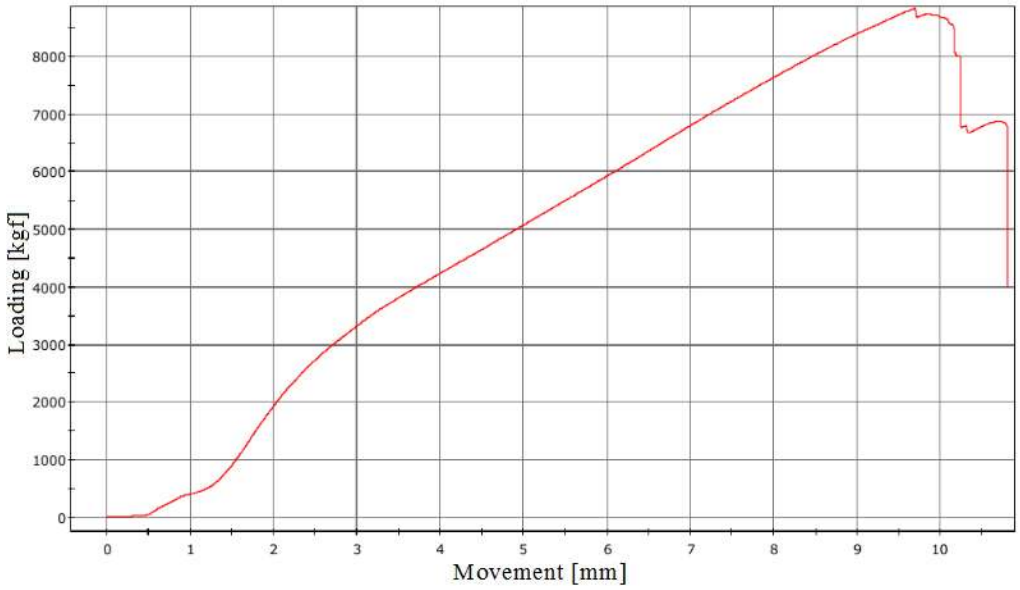


**Fig. 16.** The loading diagram for the truncated disk samples from the second group

The significant difference in the destructive forces and the localization of destruction of samples in the two groups is due to a significant difference in the type of stress state. In the first group, the stress state (with the same values of $K_\sigma$ in the first and second groups) on the surface of the concentrating groove was as “hard” as possible (Smirnov-Alyaev, 1968). For this reason, the source of crack initiation that destroyed the samples was located at the maximum point. In the second group,

the stress state was significantly "softer" with P = – 1.4. The cracks that destroyed the samples of the second group occurred on the support surface in the geometric center of this surface, in which P = 1.4. The difference in the level and type of stress state in the source of destruction of highly loaded structural elements (Zenkov & Tsvik, 2018; Zenkov & Tsvik, 2017) is typical for various machine building industries. The truncated disk samples make it possible to simplify, clarify and speed up the assessment of structural strength of the materials used in these industries and the localization and destruction of the structural elements.

## 4. Conclusion

1. The analysis revealed that the truncated samples with stress concentrators on the working surfaces (supporting surfaces or loading surfaces) used for laboratory strength testing allow for varying the level and type of stress state by changing the degree of truncation. This factor simplifies the assessment of structural strength at the stage of laboratory studies using the standard single-drive testing machines.
2. The computational experiment showed that in the studied range of dimensionless values of ρ (relative curvature of the groove surface), η (relative groove depth) and δ (truncation parameter of the sample disk), stress state type coefficient $P$ and concentration stress coefficient $K_\sigma$ change in the range of $0 \le P \le 2$; $K_\sigma < 4$. If necessary, concentrating grooves can be located on the loading surface of the samples and allow for studying the structural strength under biaxial compression.
3. The computational experiment showed that in the studied range of values of the geometric parameters of disk samples (ρ, η and δ), the dependences of $P$ and $K_\sigma$ on these parameters make it possible to simulate the values of these characteristics using the truncated disk samples.
4. For structural carbon steel St45, the experimental destruction of the disk samples revealed the determining influence of the type of stress state on the localization of the sources of destruction of supporting elements. The results of these tests can be used both for assessing the strength and constructing equations of its limit state corresponding to a given level and type of stress state.

## References


Bellett, D., Morel, F., Morel, A., & Lebrun, J. L. (2011). A biaxial fatigue specimen for uniaxial loading. *Strain*, *47*(3), 227-240.

Berto, F., Campagnolo, A., & Lazzarin, P. (2015). Fatigue strength of severely notched specimens made of Ti–6Al–4V under multiaxial loading. *Fatigue & Fracture of Engineering Materials & Structures*, *38*(5), 503-517.

Bondar, V.S., Temis, Yu.M., & Matvienko, Yu.G. (2024). *Structural strength of materials. Resource life of structures with high parameters*. St. Petersburg: Lanbook.

de Oliveira Miranda, A. C., Antunes, M. A., Alarcón, M. V. G., Meggiolaro, M. A., & de Castro, J. T. P. (2019). Use of the stress gradient factor to estimate fatigue stress concentration factors Kf. *Engineering Fracture Mechanics*, *206*, 250-266.

Drucker, D. C., & Prager, W. (1952). Soil mechanics and plastic analysis or limit design. Q. *Appl. Math*, *10*(2), 157-165.

GOST 1050-2013. (2014). *Metal products from unalloyed structural high-quality and special steels. General technical conditions*. Moscow: IKP Publishing house of standards.

GOST 1497-84. (2008). *Metals. Tensile test methods*. Moscow: IKP Publishing house of standards.

GOST 25.502-79. (1979). *Calculation and strength testing in mechanical engineering. Methods of mechanical testing of metals. Fatigue test methods*. Moscow: IKP Publishing house of standards.

GOST 25.504-82. (2004). *Calculations and strength tests. Methods for calculating the characteristics of fatigue resistance*. Moscow: IKP Publishing house of standards.

GOST 25.506-85. (1985). *Calculations and strength tests. Methods of mechanical testing of metals. Determination of crack resistance characteristics (fracture toughness) under static loading*. Moscow: IKP Publishing house of standards.

Kachanov, L. M. (2004). *Fundamentals of the Theory of Plasticity*. Courier Corporation.

Keller, I.E., & Petukhov, D.S. (2020). Criteria for strength and ductility. *Perm: Perm national research polytechnic university.*

Kogaev, V. P., Makhutov, N. A., & Gusenkov, A. P. (1985). Calculations of machine parts and structures for strength and durability. *Mashinostroenie, Moscow*.

Koutiri, I., Bellett, D., & Morel, F. (2018). The effect of mean stress and stress biaxiality in high-cycle fatigue. *Fatigue & Fracture of Engineering Materials & Structures*, *41*(2), 440-455.

Krotov, S.V., & Kononov, D.P. (2022). Analysis of the contact zone of the railway wheel and rail. *News of the St. Petersburg University of Railway Transport*, 19, 221-231.

Lebedev, A.A., & Kovalchuk, B.I. (2003). Mechanical properties of structural materials in a complex stress state. *Kiev: In Yure.*

Leevers, P. S., Radon, J. C., & Culver, L. E. (1976). Crack growth in plastic panels under biaxial stress. *Polymer*, *17*(7), 627-632.

Lurie, A. I. (2012). *Non-linear theory of elasticity*. Elsevier.

Makhutov, N. A. (1981). Deformation criteria and structural elements strength calculation. *Moscow: Mashinostroyeniye*.

Makhutov, N.A. (2005). Structural strength, service life and technogenic safety. *Novosibirsk: Science.*

Matake, T. (1977). An explanation on fatigue limit under combined stress. *Bulletin of JSME*, *20*(141), 257-263.

Mathiak, F., Krawietz, A., Nowack, H., & Trautmann, K. H. (1992). *U.S. Patent No. 5,144,844*. Washington, DC: U.S. Patent

and Trademark Office.
Neuber, G. (1947). *Stress concentration*. Leningrad: Gostehizdat.
Oden, J. (1976). *Finite elements in nonlinear continuum mechanics*. M.: Mir.
Peterson, R.E. (1977). *Stress concentration factors*. Moscow: Mir.
Pisarenko, G. S., Yakovlev, A. P., & Matveev, V. V. (2008). Materials resistance handbook. *Delta, Kiev*, *816*.
Rychkov, S.P. (2013). *Modeling of structures in the Femap with NX Nastran environment*. M.: DMK Press.
Sines, G., Waisman, J. L., & Dolan, T. J. (1959). *Metal Fatigue [by] Thomas J. Dolan [and Others] Edited by George Sines and JL Waisman*. McGraw-Hill.
Smirnov-Alyaev, G. A. (1968). Mechanical foundations of plastic processing of metals. Engineering methods. *Mechanical engineering, Leningrad*.
Tsvik, L. B. (1993). Strengthening holes and static strength of axially symmetric choke assemblies. *Problems of machine building and machine reliability*, *1*, 58-65.
Tsvik, L. B., Pimshtein, P. G., & Borsuk, E. G. (1978). Experimental study of the stress-strain state of a multilayer cylinder with a monolithic insert. *Strength of Materials*, *10*(4), 448-452.
Tsvik, L., & Zenkov, E. (2022). A comparative analysis of the stress-strain state of disc specimens in assessing the structural strength of materials. *Engineering Solid Mechanics*, *10*(1), 25-34.
Tsvik, L.B. (2017). Specimens for mechanical testing of structural steels under cyclic loading. *Transport infrastructure of the Siberian region, 2*, 834-839.
Tsvik, L.B., Mukhomedzyanov, N.S., Zenkov, E.V., & Eremeev, V.K. (2017). Discrete modeling of deformations and stresses of wheels of railway cars based on their preliminary fragmentation. *Transport infrastructure of the Siberian region*, *2*, 786–791.
Tsvik, L.B., Tarmaev, A.A., & Bocharov, I.S. (2019). Smoothness of the contours of rolling elements of bearings with cylindrical rollers and the resource of their cyclic operatio. *Transport of the Urals*, *3*(62), 20-27.
Tsvik, L.B., Zenkov, E.V., Bocharov, I..S., & Elovenko, D.A. (2020). *Patent R.F. No.2734276.* Moscow: R.F. Patent and Trademark Office.
Vilimok, Y. A., Nazarov, K. A., & Evdokimov, A. K. (2013). Stress state of flat specimens under the uniaxial and biaxial tension. *News of TSTU. Technical science*, *11*, 388-39.
Yosri, A., Zayed, A., Saad-Eldeen, S., & Leheta, H. (2021). Influence of stress concentration on fatigue life of corroded specimens under uniaxial cyclic loading. *Alexandria Engineering Journal*, *60*(6), 5205-5216.
Zenkov, E. V., & Tsvik, L. B. (2015). Formation of divergent testing efforts and experimental evaluation of material strength under biaxial stretching. *PNRPU Mechanics Bulletin*, (4), 110-120.
Zenkov, E. V., & Tsvik, L. B. (2017). Refinement of the equations of the limiting state of the structure material taking into account the real type of their deformation. *Systems. Methods. Technology*, *2*(34), 28-34.
Zenkov, E. V., & Tsvik, L. B. (2018). Accuracy improvement for combined static strength criterion for structures under complex loading. *Materials Physics & Mechanics*, *40*(1), 124-132.
Zenkov, E. V., Aistov, I. P., & Vansovich, K. A. (2019, August). Modeling stress state stiffening of the nozzle zone of pressure vessel by finite element method. In *AIP Conference Proceedings* (Vol. 2141, No. 1). AIP Publishing.
Zenkov, E. V., Tsvik, L. B., & Pykhalov, A. A. (2011). Discrete modeling of the stress-strain state of flat-cylindrical specimens with grooves as stress concentrators. *Bulletin of Irkutsk State Technical University*, *7*(54), 6-11.
Zenkov, E., & Tsvik, L. (2022, March). Modeling the Structural Strength of Materials on Disk Laboratory Specimens. In *Materials Science Forum* (Vol. 1052, pp. 104-109). Trans Tech Publications Ltd.